

Understanding coronal rain dynamics through a point-mass model

Andrew Hillier¹, Ramon Oliver^{2,3}, and David Martínez-Gómez^{4,5}

¹ Department of Mathematics and Statistics, University of Exeter, Exeter, EX4 4QF UK
e-mail: a.s.hillier@exeter.ac.uk

² Departament de Física, Universitat de les Illes Balears, E-07122, Palma de Mallorca, Spain

³ Institut d'Aplicacions Computacionals de Codi Comunitari (IAC3), Universitat de les Illes Balears, E-07122, Palma de Mallorca, Spain

⁴ Instituto de Astrofísica de Canarias, E-38205 La Laguna, Tenerife, Spain

⁵ Departamento de Astrofísica, Universidad de La Laguna, E-38205 La Laguna, Tenerife, Spain

ABSTRACT

Aims. Observations and simulations of coronal rain show that as cold and dense plasma falls through the corona it initially undergoes acceleration by gravity before the downward velocity saturates. Simulations have shown the emergence of an unexpected relation between terminal velocity of the rain and density ratio that has not been explained. Our aim is to explain this relation.

Methods. In this paper we develop a simple point-mass model to understand how the evolution of the ambient corona moving with the coronal rain drop can influence the falling motion.

Results. We find that this simple effect results in the downward speed reaching a maximal value before decreasing, which is consistent with simulations with realistic coronal rain mass. These results provide an explanation for the scaling of the maximum downward speed to density ratio of the rain to the corona and as such provide a new tool that may be used to interpret observations.

Key words. Magnetohydrodynamics (MHD) – coronal rain

1. Introduction

Quiescent coronal rain is a multiphase plasma phenomenon of cool plasma embedded in a hot component that is frequently observed in solar active regions (Antolin 2020; Antolin & Froment 2022; Şahin & Antolin 2022; Şahin et al. 2023). It starts with the continuous evaporation of cold and dense plasma from the solar chromosphere into the corona. This evaporated plasma, that now has the typical hot and rarefied conditions of the corona, accumulates at the apex of a coronal loop and eventually becomes thermally unstable (Parker 1953; Field 1965; Antiochos 1980), which leads to the formation of a dense coronal rain clump some tens of Mm high in the corona. Electron number densities of the order of $2 - 25 \times 10^{10} \text{ cm}^{-3}$ have been measured by Antolin et al. (2015), compared to characteristic coronal loops densities in active regions of the order of $1 - 10 \times 10^9 \text{ cm}^{-3}$ (Reale 2010). These values translate into clump densities of the order of $3-40 \times 10^{-14} \text{ g cm}^{-3}$ (note that post-flare coronal rain can reach higher densities; see Şahin & Antolin 2024, who report values $\sim 10^{-12} \text{ g cm}^{-3}$). After this formation phase, coronal rain falls along the loop legs toward the solar surface under the action of gravity, although in many cases it does not attain the gravitational free-fall speed, but instead reaches a constant (or even decreasing) velocity. Coronal rain typically reaches falling speeds of up to 150 km s^{-1} (see, for example, Wiik et al. 1996; Antolin & Rouppe van der Voort 2012; Kriginsky et al. 2021).

The descending phase of coronal rain is characterised by the cold and dense plasma flowing along coronal loops, which are aligned with the coronal magnetic field (see, e.g., Tripathi et al. 2006, 2007) implying that some inherent aspects of the dynamics are essentially one-dimensional (1D). This was used by Oliver et al. (2014) to set up 1D hydrodynamic models of coronal rain that reproduce the observed smaller-than-free-fall speed. These

authors also found that coronal rain blobs achieve a maximum descending velocity, after which their speed is reduced gradually in time. The work of Oliver et al. (2014) was extended to 2D by Martínez-Gómez et al. (2020). A very interesting aspect of the simulations of Martínez-Gómez et al. (2020) is that in the limit of strong magnetic field, i.e., $|B| \gtrsim 20 \text{ G}$, the simulated coronal rain dynamics effectively became the sum of a set of vertical 1D models of the type presented in Oliver et al. (2014), meaning that 1D modelling is reasonable given the strong magnetic field of the solar corona as this implies the Alfvén Mach number and plasma beta of the coronal rain is small (magnetic field strengths of the order of hundreds of Gauss or even larger have been inferred by Schad et al. 2016; Kuridze et al. 2019; Kriginsky et al. 2021). Both in Martínez-Gómez et al. (2020) and in other multi-dimensional simulations using weaker field strengths (e.g. Fang et al. 2015) it has been found that there is a greater influence of multi-dimensional effects. Assessing the dynamics of their simulated rain blobs, Martínez-Gómez et al. (2020) found, through empirical fit, that the maximum downward velocity of the falling coronal rain scales as the rain to corona density ratio to the power 0.64 (i.e. $(\rho_{\text{rain}}/\rho_{\text{corona}})^{0.64}$). A key question that still remains is: why this particular exponent?

One possible way of understanding the dynamics of these simulations may be through simplified point-mass and drag models. These models have been widely applied in many areas of fluid dynamics including the modelling of coronal mass ejection (CME) propagation (e.g. Vršnak et al. 2010, 2013). A standard aspect of drag models is that the faster the body moves, the stronger the drag force works to decelerate it. Physically, this relates to the moving structure having to do more work to push aside the ambient material as it moves faster. This model predicts a terminal fall velocity that scales (in the large density contrast

limit) as approximately the density ratio to the power 0.5 (e.g. Zhou et al. 2021). This discrepancy to the exponent found by Martínez-Gómez et al. (2020) for their simulations is interesting as it implies that some different physics needs to be considered.

Another key aspect of point-mass models, including drag models, is that as the mass moves through the medium, a portion of the ambient fluid, which will be referred to as the virtual mass, moves with the body. In effect, this adds to the mass of the moving body. For a standard drag problem, including one that involves incompressible flow, the virtual mass of the system is expected to not change significantly over time (e.g. as used in Vršnak et al. 2010, 2013). If the mass of the body is larger than that of the virtual mass, then the virtual mass does not change the dynamics in any significant way. Due to the high mass of a coronal rain blob, we may naturally expect this to be the case. However, this assumption may not hold for the coronal rain falling along magnetic field as a significant amount of material in front of and behind the moving coronal rain has to move as well.

In this paper we develop a simple model for the coronal rain dynamics simulated by Oliver et al. (2014) and Martínez-Gómez et al. (2020) looking at the role of virtual mass to quantify how it controls the evolution of the rain motion. We then use this model to provide an explanation for the density and coronal rain velocity scaling presented in Martínez-Gómez et al. (2020).

2. An overview of the numerical modelling

We consider a one-dimensional vertical slice of a fully ionised hydrogen plasma. The adiabatic hydrodynamic evolution of this system is described by the continuity equations of mass, momentum and pressure:

$$\frac{\partial \rho}{\partial t} = -v \frac{\partial \rho}{\partial z} - \rho \frac{\partial v}{\partial z}, \quad (1)$$

$$\rho \frac{\partial v}{\partial t} = -\rho v \frac{\partial v}{\partial z} - \frac{\partial p}{\partial z} - \rho g, \quad (2)$$

$$\frac{\partial p}{\partial t} = -v \frac{\partial p}{\partial z} - \gamma p \frac{\partial v}{\partial z}. \quad (3)$$

Here t and z are time and the vertical coordinate, with the z -axis pointing upward; $\rho(z, t)$, $v(z, t)$ and $p(z, t)$ are the density, vertical velocity component and pressure; $g = 274 \text{ m s}^{-2}$ is the acceleration of gravity at the solar surface; and $\gamma = 5/3$ is the ratio of specific heats.

In an isothermal atmosphere with temperature T_0 the plasma is in hydrostatic equilibrium with pressure and density given by

$$p(z) = p_0 \exp\left(-\frac{z}{H}\right), \quad (4)$$

$$\rho(z) = \rho_0 \exp\left(-\frac{z}{H}\right), \quad (5)$$

where the vertical scale-height H is

$$H = \frac{2k_B T_0}{m_p g}, \quad (6)$$

with k_B the Boltzmann constant and m_p the proton mass. To derive Equation 6 we have used the perfect gas law for a fully ionised hydrogen gas,

$$p_0 = 2 \frac{k_B}{m_p} \rho_0 T_0. \quad (7)$$

Now, we study the temporal evolution of the system with zero initial velocity, initial pressure given by Equation 4 and initial density given by the sum of Equation 5 plus a blob density,

$$\rho_b(z) = \rho_{b0} \exp\left[-\left(\frac{z-z_0}{\Delta}\right)^2\right]. \quad (8)$$

To obtain $\rho(z, t)$, $v(z, t)$ and $p(z, t)$ we perform numerical simulations as described in Oliver et al. (2014). The problem parameters are the background homogeneous temperature, T_0 , the density at the $z = 0$ height, ρ_0 , the initial height of the dense blob, z_0 , and the blob density and length, ρ_{b0} and Δ . The pressure at the $z = 0$ height, p_0 , appears in Equation 4 and can be determined from T_0 and ρ_0 with the help of Equation 7. With no loss of generality, we set $\rho_0 = 5 \times 10^{-12} \text{ kg m}^{-3}$ and $z_0 = 50 \text{ Mm}$. Hence, we are left with three free parameters, namely T_0 (or H), ρ_{b0} and Δ .

The temporal evolution of the system is as follows: the introduction of a density enhancement at $z = z_0$ sends two sound waves travelling up and down at the (constant) sound speed $C_s = \sqrt{\gamma p_0 / \rho_0}$. The blob also starts to fall with a subsonic speed (see Figure 1(a) and the corresponding movie) until it reaches a maximum downward velocity, $v_{b,\text{max}}$, after which it presents a gentle deceleration. This behaviour of the blob velocity is shown in Figures 2(a), (b), (c). Oliver et al. (2014) found an unexpected association between $v_{b,\text{max}}$ and the ratio of the blob density to the local ambient density at $t = 0$; here we denote this density ratio as dr . This association is surprising because atmospheres with different T_0 have different scale heights and, although the blob falls through atmospheres with different stratification, it appears that only the initial ambient density at height z_0 matters. The plot of $v_{b,\text{max}}$ versus dr in Oliver et al. (2014) was presented for $\Delta = 0.5 \text{ Mm}$. Changes to this parameter lead to increases or decreases of the blob mass and, therefore, to larger or smaller $v_{b,\text{max}}$, respectively, and the already mentioned association is not fulfilled. To correct for this fact, one can plot $v_{b,\text{max}}$ as a function of Δdr , as shown in Figure 2(d), which results in the points aligning relatively neatly along a curve with little, but non-negligible, spread.

In addition, the falling blob pushes down the gas below it and also pulls down the gas above it. In other words, part of the vertical mass column is set into motion because of the presence of the density enhancement. The lower and upper points of this mass column travel at speed C_s , hence at time t they have coordinates $z = z_0 \pm C_s t$ (see Figure 1(b) and the corresponding movie). The two boundaries of the numerical domain are placed at a large distance from the initial blob position and this prevents the sound waves that bounce off the boundaries from interfering with the blob dynamics (for more details, see Oliver et al. 2014).

3. The importance of virtual mass

Our aim in this paper is to develop a simple analytic model for the motion of coronal rain as presented in the simulations of Oliver et al. (2014) and Martínez-Gómez et al. (2020). Having seen from the simulations presented in Section 2 that a large region of the corona responds to the motion of the coronal rain, see Figure 1(b), the implication of this is that the ambient mass (i.e. the virtual mass) is evolving and can be significant. Therefore, the key question we need to determine first is: What might be the virtual mass for our problem? There are two key pieces of information from the works of Oliver et al. (2014), Martínez-Gómez et al. (2020) and Section 2 that we will use: 1) that if we have a

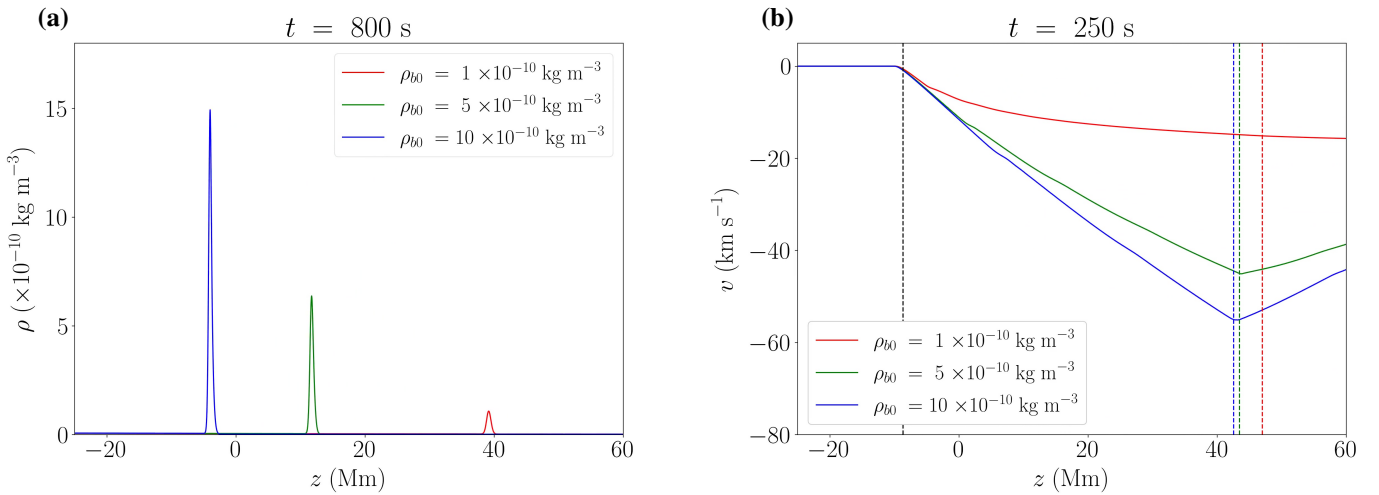


Fig. 1: Results of three numerical simulations with $T_0 = 2 \times 10^6$ K, $\Delta = 0.5$ Mm and $\rho_{b0} = 10^{-10}$ kg m $^{-3}$ (red), $\rho_{b0} = 5 \times 10^{-10}$ kg m $^{-3}$ (green) and $\rho_{b0} = 10 \times 10^{-10}$ kg m $^{-3}$ (blue). (a) Density as a function of height at a given time. (b) Velocity as a function of height at a given time. A dashed black vertical line is plotted at $z = z_0 - C_s t$ giving the position of the front of the compression wave. The red, green and blue dashed vertical lines give the position of the maximum density. Animations of these figures can be found online.

strong magnetic field, the 2D dynamics becomes 1D like, therefore we only look to model 1D dynamics using a point mass, and 2) that two waves, a compression wave propagating downward and a rarefaction wave propagating upward, are set off as the blob starts to move. The fronts of these waves propagate at the sound speed of the ambient medium. The distance these wave fronts have propagated at a given time determines the amount of the ambient mass (i.e. the virtual mass) that can respond to the motion. The growth of the virtual mass in time can be seen in Figure 1(b) and the accompanying movie, in which the vertical black line separates the unperturbed and perturbed plasma below and above this height, respectively. As time evolves, the height represented by the vertical line moves down at the constant speed C_s . This means that unlike a standard drag model the virtual mass evolves over time.

This leads to the question: How can we include this dynamically evolving virtual mass into a simple drag-like model? If we treat our coronal rain blob as a mass (m_b) falling through a vacuum, then we get this simple equation for the dynamics

$$m_b \frac{dv_b}{dt} = -m_b g. \quad (9)$$

But what happens with the virtual mass (m_v) is that it takes momentum from the coronal rain and puts it into the surrounding material. Treating the virtual mass as being able to respond instantly to changes in the momentum of the blob, we need to add two terms to Equation 9: one to show how change in the speed of the blob increases the speed of the virtual mass, and another one to represent the change in the virtual mass, because it is a growing region due to the continued propagation of the sound waves, increasing the momentum of the virtual mass (and reducing the momentum of the blob). This leads to

$$m_b \frac{dv_b}{dt} = -m_b g - m_v \frac{dv_v}{dt} - v_v \frac{dm_v}{dt}, \quad (10)$$

where v_v is the velocity of the virtual mass.

Now, we don't know v_v (in fact, as with v_b , it will not be a single value but we treat it as such - this can be seen by the

broad velocity distributions in Figure 1b going from zero at the compression wave front to a maximum at the blob position), and as it relates to how the mass in front of and behind the blob moves, it will be some factor (which may not be constant) of the blob velocity which we denote $D(t)$. This means we represent the average speed of the material in front of and behind the moving blob as $D(t)v_b$. This gives:

$$m_b \frac{dv_b}{dt} = -m_b g - m_v \frac{d}{dt}(D(t)v_b) - D(t)v_b \frac{dm_v}{dt}, \quad (11)$$

or

$$\frac{d}{dt}((m_b + D(t)m_v(t))v_b) = -m_b g, \quad (12)$$

where we assume that the coronal rain mass (m_b) is constant. Note that Equation 12 does not include any drag term, and can be used to get a formula for the velocity at a given time. This latter formula is

$$v_b = -\frac{m_b g}{m_b + D(t)m_v(t)} t. \quad (13)$$

So now we look at some specific situations for understanding the evolution of the virtual mass and how this influences the dynamics. We note here that we will take $D(t)$ to be a constant D for the rest of this section. We will then be able to check the validity of this assumption when comparing to simulation results.

3.1. Virtual mass in a constant density background

Before looking at a stratified atmosphere, it is informative to look at the case of a constant density background (ρ_0) with a constant sound speed (C_s). We have the mass of the blob given by $m_b = S F_b \rho_0 h_b$, where ρ_0 is the density of the corona where the blob is placed, F_b is the increase factor of the density, S is the cross-sectional area and h_b is a measure of the blob length (to take this from density to mass). The conversion between Δ (the half-width of the Gaussian distribution) in Oliver et al. (2014) and this model is $h_b = \sqrt{\pi} \Delta$ as this means the value of F_b used

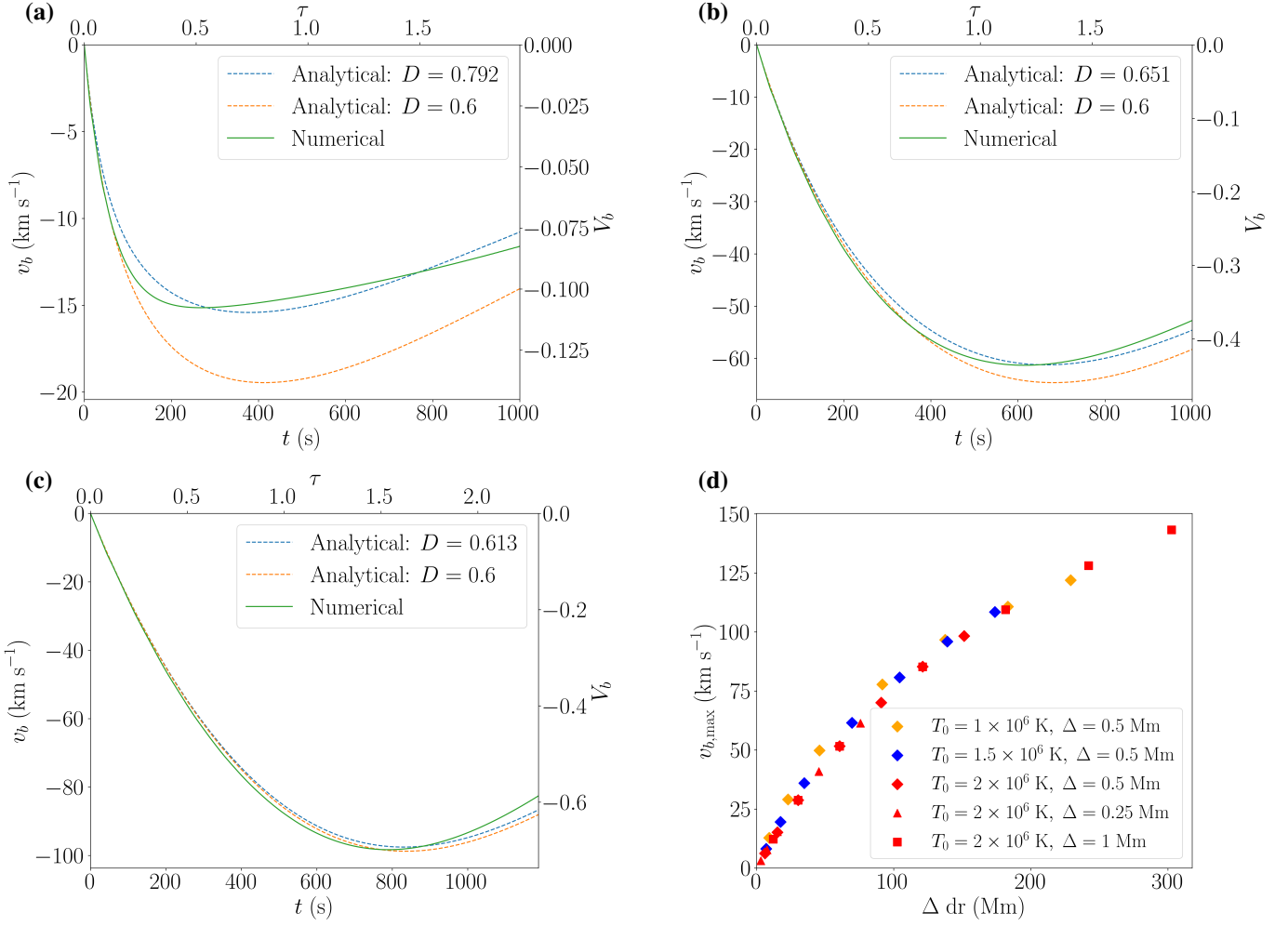


Fig. 2: Blob velocity as a function of time for three setups with $T_0 = 2 \times 10^6$ K, $\Delta = 0.5$ Mm and (a) $\rho_{b0} = 10^{-10}$ kg m⁻³, (b) $\rho_{b0} = 5 \times 10^{-10}$ kg m⁻³ and (c) $\rho_{b0} = 10 \times 10^{-10}$ kg m⁻³. The green curve comes from the numerical solution of Equations 1–3, whereas the analytical approximation of Equation 18 is given by the blue and orange curves for the best fit of D and for $D = 0.6$, respectively. The variables τ and V_b are the dimensionless time and blob speed (see Section 3.2). (d) (Unsigned) maximum blob velocity, $v_{b,max}$, versus Δdr (the meaning of the different symbols is given in the figure legend).

here directly relates to the density ratio of Oliver et al. (2014) and the simulations of Section 2. For the virtual mass, we know that the mass in causal contact with the moving blob can be given by

$$m_v = 2S\rho_0 C_s t. \quad (14)$$

Based on these arguments we have

$$v_b = -\frac{g}{1 + \frac{2DC_s t}{F_b h_b}} t. \quad (15)$$

We can quickly see that at early times, the downward velocity will increase at an approximately linear rate which is consistent with free-fall. However, at late times the denominator will approximately scale linearly with time leading to the downward velocity converging to a value of

$$v_b(\text{final}) = -\frac{gF_b h_b}{2DC_s}. \quad (16)$$

This simple model shows we expect the final velocity to be linearly proportional to the density ratio. However this does not have the earlier peak in velocity with a slow decline afterwards that is seen in Figure 2.

3.2. Virtual mass in a stratified atmosphere

Our next step is to develop the model to include a stratified atmosphere with constant sound speed to mimic the simulations presented in Section 2. This leads to a more complex evolution of the virtual mass. Setting the position where the blob is placed to be $z = 0$ we then have

$$\begin{aligned} m_v &= \rho_0 S \int_{-C_s t}^{C_s t} \exp(-z/H) dz \\ &= H\rho_0 S \left[\exp\left(\frac{C_s t}{H}\right) - \exp\left(-\frac{C_s t}{H}\right) \right] = 2H\rho_0 S \sinh\left(\frac{C_s t}{H}\right), \end{aligned} \quad (17)$$

with H as the pressure scale height. Justification for this range of integration is shown in Figure 1(b) which shows that for any initial coronal rain mass the region of the ambient corona that is influenced by its motion is restricted to the regions in causal contact as determined by the propagation of the front of the compression and rarefaction waves which travels at the ambient sound speed. With this new formula for the virtual mass, this

gives us

$$v_b = -\frac{g}{1 + \frac{2D(t)H}{F_b h_b} \sinh\left(\frac{C_s t}{H}\right)} t. \quad (18)$$

As $t/\sinh(C_s t/H)$ tends to zero as t tends to infinity this implies that v_b will tend to zero at large times. However, for small (but non-zero) t we have a situation that is equivalent to the constant density case so the the downward velocity will initially increase in magnitude with $v_b \propto t$.

The results from this model are overplotted as the orange and blue dashed lines in Figures 2(a), (b), (c). The blue dashed line is the solution for a value of D optimised to give the best fit to $v_b(t)$, the orange line is for a value of $D = 0.6$. Both these curves give acceleration of the coronal rain downwards and then deceleration as the virtual mass becomes significant. We can see in Figures 2(a), (b), (c) that as the mass of the coronal rain is increased, the simulation results become closer to those of the $D = 0.6$ curve. The value of $D = 0.6$ implies that the average velocity of the virtual mass is more weighted to the blob mass than would be found for a linear velocity profile. The velocity profiles in Figure 1 (b) show that such a profile is found in the simulations.

To make further progress (i.e. to remove the temperature effects from the equation), we can non-dimensionalise Equation 18. Firstly we set $\tau = C_s t/H$. This gives (taking D to be constant)

$$v_b = -\frac{gH/C_s}{1 + \frac{2DH}{F_b h_b} \sinh(\tau)} \tau. \quad (19)$$

From this equation we see we have the freefall velocity after a sound crossing time (gH/C_s) and the ratio of the blob mass to the mass in a pressure scale height ($M = F_b h_b/H$) as fundamental quantities of the system. This leads to the non-dimensionalised equation

$$V_b = -\frac{1}{1 + \frac{2D}{M} \sinh(\tau)} \tau, \quad (20)$$

with $V_b = v_b C_s/(gH)$.

The next step is to determine the relation between M and the maximum value of V_b ($V_{b,\max}$). By taking the derivative of Equation 20 with respect to τ , we find

$$M = 2D \cosh(\tau_{\max})(\tau_{\max} - \tanh(\tau_{\max})), \quad (21)$$

with τ_{\max} the value of τ associated with $V_{b,\max}$. Using this to remove M from Equation 20 gives

$$V_{b,\max} = \tau_{\max} - \tanh(\tau_{\max}). \quad (22)$$

Though this does not give a direct analytic formula for dependence of $V_{b,\max}$ on M , it does allow them to be directly connected.

The simulation results are plotted using this new normalisation in Figure 3. This shows the various different models collapsed onto the same curve, confirming that the non-dimensionalisation correctly captures the underlying physics of the problem. The dashed line is the analytic prediction stated above using $D = 0.6$. We can see that at small M the model slightly over-predicts the value of $V_{b,\max}$. However, above $M \approx 1$, the simulation results and the model align to good degree. It should also be noted that using the normalisation in this figure, the small spread that can be seen in the simulation results presented in Figure 2(d) has been completely removed.

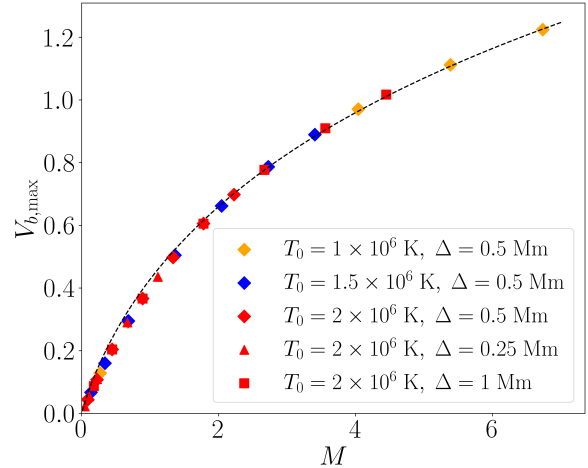


Fig. 3: Plot of (unsigned) maximum V_b against M for the simulation results (the meaning of the different symbols is given in the figure legend). The dashed line is the predicted value from Equation 20 with $D = 0.6$.

4. Summary and discussion

In this paper, we have presented a simple model for the dynamics of coronal rain that provides an explanation of much of the behaviour found in the simulations of rain evolution by Oliver et al. (2014). The key process is that the corona responds over a large distance (determined by the propagation of sound waves) to the motion of the coronal rain to effectively add mass to the system which in turn reduces its speed. A particular key result is that the scaling of the maximum downflow speed as a function of the density ratio to the power 0.64 given by a fit to the data in Martínez-Gómez et al. (2020) here is explained by an analytic relation that appears to have a similar trend to this power law.

As we have been able to show that the model for virtual mass effectively decelerating the coronal rain in the model of Oliver et al. (2014), this leads to the question: what role if any does a drag-like (by this we mean a term $\propto v_b^2$) play? In fact we can see in Figure 3 that for small M values, the value of $V_{b,\max}$ from the simulations is smaller than we predict from our model. For these small-mass cases, it is likely that pressure gradients acting to give an upward force are created by the downward motion of the coronal rain and these can act as a drag. However, for larger rain mass (i.e. $M \gtrsim 1.5$ which are more consistent with those of the solar atmosphere) this effect becomes small.

Finally, an important question to ask is: can we reasonably assume that $D(t)$ will be constant in time, and will it have the same value for the regions above and below the coronal rain. We can see from Figure 2 that for large rain mass the model provides a good representation of the velocity evolution over long time (i.e. $M \gtrsim 1.5$ the lower bound of which corresponds to Figure 2(b)), meaning that changes in the value should be small. However, at very large (i.e. $M \gtrsim 6$) rain masses the downflow velocity may become trans- or super-sonic which will change the way in which the rain motion is transmitted into the surrounding corona. This will likely result in the value of D evolving over time. Relevant to this, some observations have implied that there is strong compression (Antolin et al. 2023) or shocks (Schad et al. 2016) preceding coronal rain blobs. Compression in front of the rain as it moves is a fundamental aspect of our

model. Therefore, observations may create a pathway to calculate the value of D for real dynamics. In addition to this, shock formation is something that our model implies as a possibility and an important further step will be calculating the relevant M values for the observations to see if we are predicting transonic flow.

As a final comment, simplified drag models are widely used in understanding and modelling dynamics in a broad range of situations including CME propagation (e.g. Vršnak et al. 2010) and the dynamics of cool, dense clouds of gas in fast outflows found in the Intracluster medium (e.g. Gronke & Oh 2018). However, our model with evolving virtual mass is more relevant for situations with strong magnetic field, as quantified by having sub-Alfvénic flow speeds in a low-beta plasma environment. This is a fundamental difference from the examples listed above where weaker magnetic fields mean aerodynamic drag is the dominant process influencing the temporal evolution. As such, the ideas that underpin our model are likely to be applicable in situations where motion is confined to flow along the magnetic field; an example of this may be accretion to the poles of highly magnetised neutron stars (e.g Davidson 1973), presenting some further avenues for this work.

Acknowledgements. AH is supported by STFC Research Grant No. ST/R000891/1 and ST/V000659/1. DM acknowledges support from the Spanish Ministry of Science and Innovation through the grant CEX2019-000920-S of the Severo Ochoa Program. This publication is part of the R+D+i project PID2023-147708NB-I00, financed by MICIU/AEI/10.13039/501100011033/ and FEDER, EU. AH and RO would like to acknowledge the discussions with members of ISSI Team 457 “The Role of Partial Ionization in the Formation, Dynamics and Stability of Solar Prominences” and ISSI Team 545 “Observe Local Think Global: What Solar Observations can teach us about Multiphase Plasmas across Astrophysical Scales”, which have helped improve the ideas in this manuscript. We would also like to thank the anonymous referee for their useful comments. The simulation data presented in Section 2 is based on the work of Oliver et al. (2014) and will be made available on reasonable request. There are no other data produced for this paper.

References

- Antiochos, S. K. 1980, ApJ, 241, 385
 Antolin, P. 2020, Plasma Physics and Controlled Fusion, 62, 014016
 Antolin, P., Doliou, A., Auchère, F., et al. 2023, A&A, 676, A112
 Antolin, P. & Froment, C. 2022, Frontiers in Astronomy and Space Sciences, 9, 820116
 Antolin, P. & Rouppe van der Voort, L. 2012, ApJ, 745, 152
 Antolin, P., Vissers, G., Pereira, T. M. D., Rouppe van der Voort, L., & Scullion, E. 2015, ApJ, 806, 81
 Şahin, S. & Antolin, P. 2022, ApJ, 931, L27
 Şahin, S. & Antolin, P. 2024, ApJ, 970, 106
 Şahin, S., Antolin, P., Froment, C., & Schad, T. A. 2023, ApJ, 950, 171
 Davidson, K. 1973, Nature Physical Science, 246, 1
 Fang, X., Xia, C., Keppens, R., & Doorselaere, T. V. 2015, The Astrophysical Journal, 807, 142
 Field, G. B. 1965, ApJ, 142, 531
 Gronke, M. & Oh, S. P. 2018, MNRAS, 480, L111
 Kriginsky, M., Oliver, R., Antolin, P., Kuridze, D., & Freij, N. 2021, A&A, 650, A71
 Kuridze, D., Mathioudakis, M., Morgan, H., et al. 2019, ApJ, 874, 126
 Martínez-Gómez, D., Oliver, R., Khomenko, E., & Collados, M. 2020, A&A, 634, A36
 Oliver, R., Soler, R., Terradas, J., Zaqarashvili, T. V., & Khodachenko, M. L. 2014, ApJ, 784, 21
 Parker, E. N. 1953, ApJ, 117, 431
 Reale, F. 2010, Living Reviews in Solar Physics, 7, 5
 Schad, T. A., Penn, M. J., Lin, H., & Judge, P. G. 2016, ApJ, 833, 5
 Tripathi, D., Solanki, S. K., Mason, H. E., & Webb, D. F. 2007, A&A, 472, 633
 Tripathi, D., Solanki, S. K., Schwenn, R., et al. 2006, A&A, 449, 369
 Vršnak, B., Žic, T., Falkenberg, T. V., et al. 2010, A&A, 512, A43
 Vršnak, B., Žic, T., Vrbanec, D., et al. 2013, Sol. Phys., 285, 295
 Wiik, J. E., Schmieder, B., Heinzel, P., & Roudier, T. 1996, Sol. Phys., 166, 89
 Zhou, Y., Williams, R. J. R., Ramaprabhu, P., et al. 2021, Physica D Nonlinear Phenomena, 423, 132838